Pacific Northwest
NATIONAL LABORATORY

PNNL-39005

An Infrared Database of n/k Optical Constants for Calculating Aerosol Spectra for the PICARD Program

Final Report

December 2025

Tracy Baker, Thomas Blake, Jeremy Erickson, Timothy Johnson, Schuyler Lockwood, Tanya Myers

U.S. DEPARTMENT of ENERGY

Prepared for the U.S. Department of Energy
under Contract DE-AC05-76RL01830

DISCLAIMER

PACIFIC NORTHWEST NATIONAL LABORATORY
operated by
BATTELLE
for the
UNITED STATES DEPARTMENT OF ENERGY
under Contract DE-AC05-76RL01830

Printed in the United States of America

Available to DOE and DOE contractors from
the Office of Scientific and Technical Information,
P.O. Box 62, Oak Ridge, TN 37831-0062
www.osti.gov
ph: (865) 576-8401
fox: (865) 576-5728
email: reports@osti.gov

Available to the public from the National Technical Information Service
5301 Shawnee Rd., Alexandria, VA 22312
ph: (800) 553-NTIS (6847)
or (703) 605-6000
email: info@ntis.gov
Online ordering: http://www.ntis.gov

PNNL-39005

An Infrared Database of n/k Optical Constants for Calculating Aerosol Spectra for the PICARD Program

Final Report

December 2025

Tracy Baker, Thomas Blake, Jeremy Erickson, Timothy Johnson, Schuyler Lockwood, Tanya Myers

Prepared for
the U.S. Department of Energy
under Contract DEAC0576RL01830

Pacific Northwest National Laboratory
Richland, Washington 99354

Abstract

The objective of the PICARD Program is to develop fieldable sensing platforms for the rapid chemical identification of aerosol particles in plumes. Standoff detection involves interrogating the aerosol cloud from a distance using optical methods and probing the signal returned from direct backscattering from the aerosol particles or transmitted through the plume after reflection from a retroreflector or surface of opportunity (SOO). The identification of chemical species, in aerosols, however, is complicated by their complex compositions and morphologies, chemical interferants, and non-uniform particle sizes. To advance standoff detection of aerosols, modeling the infrared transmittance, reflectance, and scattering spectra of aerosolized liquid and solid chemical compounds is required, and then testing that model experimentally via laboratory and field experiments. To perform accurate modeling, the infrared optical constants (*n*/*k*), i.e., the complex refractive index, of the compounds of interest are required. Thus, PNNL was tasked to provide the optical constants for a set of analytes relevant to the PICARD program. This report describes the experimental techniques used to derive the optical constants of both liquid and solid compounds using established "gold-standard" protocols, how the experimental data are processed to produce the wavenumber (cm^{-1}) dependent optical constant vectors, and how the data are used in the aerosol absorption spectra modeling.

For liquid compounds, absorption spectra are recorded by injecting the liquid of interest into infrared transmission cells that have various micron-scale path lengths. Spectra of the cells are recorded between 10,000 and 400 cm^{-1} using FTIR spectroscopy. About ten different cell path lengths are used to optimize signal-to-noise for both weak and strong spectral features, and a composite infrared absorption spectrum is constructed from the path length-burdens. A measurement of the refractive index of the liquid in the visible and near infrared establishes an "anchor" point for the real index of the liquid. The index value and absorption spectrum of the liquid are used as inputs to a Kramers-Kronig transform to produce the *n* and *k* vectors for the liquid.

For solid chemical compounds, the infrared optical constants are measured in one of three ways. (1) For most of the solid materials, the analyte compound is carefully weighed and mixed with a known amount of potassium bromide (typically less than 1 wt% analyte in KBr). Several weight percent samples are made for a given analyte, and then the infrared transmission spectra are measured. From the optical depth of each pellet and the infrared spectra, the absorption coefficient of the analyte is determined, and from that the *k* vector can be derived. A

Kramers-Kronig transform is then performed on the *k* vector to determine the *n* vector. (2) For samples that do not have significant absorption features in the infrared or undergo chemical conversion with KBr, single-angle reflectance spectroscopy is used. For this method, the compound is finely ground and then pressed into a (neat) 13 mm pellet using a hydraulic press. The pellet is then placed at the focus of a single angle reflectance accessory, and the reflectance spectrum is recorded from 7800 to 0 cm^{-1} by optimizing the FTIR components and using mathematical extrapolation. The reflectance spectrum is then passed through a Kramers-Kronig transform to produce the *n/k* vectors. (3) Spectroscopic ellipsometry is another method for measuring the *n* and *k* vectors of a solid compound. Because this method requires considerable signal averaging and data processing, this technique is primarily used for confirming the *n* and *k* values measured by one of the other methods.

To advance optical detection of aerosols, transmittance, reflectance, and scattering spectra for an ensemble of aerosol particles are needed, including data for different particle sizes, types, and concentrations. PNNL developed software to model the IR scattering, transmittance (T) and absorbance (A) of liquid aerosols for target species and background materials, such as water or solids (e.g., carbon soot). Since the amount of reflected, refracted, transmitted, or scattered light (as a function of wavelength) depends on the sample geometry, spectra were modeled for typical size distributions using a series of size diameters (e.g., 1, 2, 5, 10 µm, etc.). Additionally, the model can accommodate mixed chemical species with distinct refractive indices.

The final section of this report lists the liquid and solid compounds for which PNNL measured and delivered *n* and *k* vectors to the PICARD program.

Acknowledgments

The research is based upon work supported by the Office of the Director of National Intelligence (ODNI), Intelligence Advanced Research Projects Activity (IARPA), via DOE DE-AC05-76RL01830. The views and conclusions contained herein are those of the authors and should not be interpreted as necessarily representing the official policies or endorsements, either expressed or implied, of the ODNI, IARPA, or the U.S. Government. Pacific Northwest National Laboratory is operated by Battelle for the U.S. Department of Energy.

Acronyms and Abbreviations

A	absorbance
A	first Sellmeier coefficient
A_{10}	log base10 absorbance of light in a material
APS	aerodynamic particle sizer
B	second Sellmeier coefficient
C	third Sellmeier coefficient
CAS	chemical abstract service
cm^{-1}	wavenumber of light; it is the reciprocal of the wavelength of light in centimeters
CWA	chemical weapons agent
d	optical depth
DEP	diethyl phthalate
DOS	dioctyl sebacate
DLaTGS	deuterated lanthanum α-alanine-doped triglycine sulfate
DTGS	deuterated triglycine sulfate
FTIR	Fourier transform infrared
FDTD	finite difference time domain
Ge/CaF_2	germanium/calcium fluoride beamsplitter
Ge/KBr	germanium/potassium bromide beamsplitter
GUI	graphical user interface
$I(\tilde{\nu})$	intensity of light emerging a material
$I_0(\tilde{\nu})$	intensity of light incident on a material
IR	infrared
IRSE	infrared spectroscopic ellipsometry
$k(\tilde{\nu})$	imaginary part of a material's index of refraction

$K(\tilde{\nu})$	absorption coefficient
KBr	potassium bromide
KKT	Kramers-Kronig transform
LZKKTB	a FORTRAN program that carries out a Kramers-Kronig transform on an input spectral file
µm	micron
MIR	mid-infrared
$n(\tilde{\nu})$	real part of a material's index of refraction
nm	nanometer
$\tilde{\nu}$	wavenumber in cm^{-1}
NIR	near-infrared
OPS	optical particle sizer
$\mathcal{P}$	Cauchy principal value
PBA	pharmaceutical-based agent
$\phi(\tilde{\nu})$	phase angle
PICARD	Pursuing Intelligent Complex Aerosols for Rapid Detection
PNNL	Pacific Northwest National Laboratory
$R(\tilde{\nu})$	reflectance
r	pellet radius
ρ	analyte density in pellet
SA	single angle
SNR	signal-to-noise ratio
T	transmittance
txt	text file extension
UV	ultraviolet

Table of Contents

AN INFRARED DATABASE OF N/K OPTICAL CONSTANTS FOR CALCULATING AEROSOL SPECTRA FOR THE PICARD PROGRAM 1.0

ABSTRACT II

ACKNOWLEDGMENTS II

ACRONYMS AND ABBREVIATIONS V

FIGURES VIII

TABLES X

1.0 INTRODUCTION 1

2.0 EXPERIMENTAL 2

2.1 LIQUIDS 2
2.2 SOLIDS 3

3.0 DATA REDUCTION 5

3.1 LIQUIDS 5
3.2 SOLIDS 7

4.0 RESULTS 12

4.1 OPTICAL MODELING 12

5.0 DELIVERABLE 16

6.0 REFERENCES 20

Figures

Figure 1. A schematic depicting the calculations needed for estimating the transmittance spectra for an ensemble of different size particles in a) the case of liquid droplets of the same medium (i.e., the same refractive index); and b) the case of particles of different liquids, (i.e., different refractive indices). For liquids with larger k-values, longer optical paths correspond to greater attenuation at those wavelengths.

Figure 2. Liquid absorbance spectra are measured using a Fourier transform infrared spectrometer (upper left). Spectra are recorded with the liquid in a series of cells with different path lengths (lower left). Absorbance spectra, $A_{10}(\tilde{\nu}) = -\log_{10}\left(\frac{I(\tilde{\nu})}{I_0(\tilde{\nu})}\right)$, of silicon oil in two different wavenumber ranges are shown (middle). From these absorbance spectra, a composite *k* spectrum is calculated. Using a refractometer (upper right), an *n* value of the liquid at 1.55 mm is measured, and this, along with the k spectrum is used to calculate the *n* spectrum (lower right).

Figure 3. Absorbance spectra of 3-bromotoluene measured with a 500 µm cell and instruments configured for the NIR (top trace) and MIR (bottom trace) spectral range. Only the NIR data are used in this spectral region to provide good SNR. Spectra are vertically offset for clarity.

Figure 4. The infrared variable angle spectroscopic ellipsometer is shown on the left. The Bruker A510 single angle (11°) specular reflectance accessory, used for the single angle reflectance measurements, is shown in the middle two panels. A pelletized organic material is shown in the panel at the right. Organic material is ground and pressed into a pellet that is 13 or 20 mm in diameter. These pellets can then be put into the sample holder of the A510. Pellets made predominantly of KBr (< 1% analyte) can be used for the absorption method.

Figure 5. Multi-burden absorbance spectra (3400 - 2400 cm^{-1}) of silicone oil for varying cell path lengths (1 – 1006 µm). For the long path lengths, the data become nonlinear for ABS ~> 2. The dashed lines represent spectral regions where different cell path lengths were used to generate the composite spectrum.

Figure 6. Plot of the measured refractive index values (blue symbols) versus the modified Sellmeier fit (orange trace) for silicone oil.

Figure 7. $n(\tilde{\nu})$ and $k(\tilde{\nu})$ of silicon oil using 10 liquid cell path lengths ranging from 1 to 1006 µm.

Figure 8. Plot of the absorption coefficient, $K(\tilde{\nu})$, for metformin calculated for four different KBr pellets measured in the mid-infrared (_M) and the near-infrared (_N).

Figure 9. The calculated infrared optical constants for metformin are shown. The optical constants were determined by measuring the absorbance spectra of metformin-

in-KBr pellets, calculating a *k* spectrum, and then using a Kramers-Kronig transform to calculate *n*.

Figure 10. The reflectance spectrum of a UV-grade, fused silica window (CVI Laser Optics, Inc. part number PW1-1525-UV) is shown.

Figure 11. The n/k vectors shown in the plot were generated by performing a Kramers-Kronig transform on the reflectance spectrum shown in Fig. 10.

Figure 12. The plot shows the *n/k* vectors for UV-grade fused silica as determined from single angle reflectance and variable angle spectroscopic ellipsometry. The *n* vectors (left axis linear scale; blue and pink traces) show excellent agreement. The *k* vectors (right axis logarithmic scale; red and orange traces) show excellent agreement below 1800 cm^{-1} for larger *k* values. The ellipsometric technique is more sensitive to weaker *k* values and structure in the *k* vector above 1800 cm^{-1}.

Figure 13. Predicted transmittance from 7 to 10 μm for a 10 μm particle of diethyl phthalate (DEP) using finite difference time domain (FDTD) (orange) and the PNNL Mie scattering-based software (green) compared to a 10 μm slab of DEP (blue).

Figure 14. Optical constants for liquid dioctyl sebacate with the *k* (imaginary) and *n* (real) values plotted on same axis from 10,000 – 400 cm^{-1} (1 – 25 μm).

Figure 15. Left: Modeled total scattered light intensity using aerodynamic (red) or optical (blue) particle diameter distributions for the nebulized DOS aerosol sample compared to transmittance for a 10 μm slab (orange). Right: Aerodynamic (red) and optical (black) particle diameter distributions for a nebulized dioctyl sebacate DOS aerosol sample.

Tables

Table 1. Pellets prepared in KBr for measurements of metformin.

Table 2. PICARD chemical list for *n*/*k* measurements.

1.0 Introduction

The Pursuing Intelligent Complex Aerosols for Rapid Detection (PICARD) program develops advanced technologies to measure and analyze aerosols, including from standoff distances. [1] This includes not only identification of aerosol size and morphology, but also chemical composition. One of the most powerful methods to achieve this goal is infrared (IR) or near-infrared (NIR) spectroscopy to measure the spectrum of the aerosol ensemble, at standoff distances of meters to hundreds of meters. [2-7] However, because it is not possible to measure the millions of spectra that would represent all permutations of different aerosol compositions, morphologies and sizes, it is more realistic to calculate the associated spectra using, for example, the Fresnel equations, the Beer-Lambert law of light absorption, etc. [8-15] All such calculations are predicated, however, on having the *n/k* optical vectors on hand [15-17] where *n* is the real and *k* is the imaginary component of complex refractive index. PNNL has been tasked to provide such optical reference data to the PICARD program (see Figure 1).

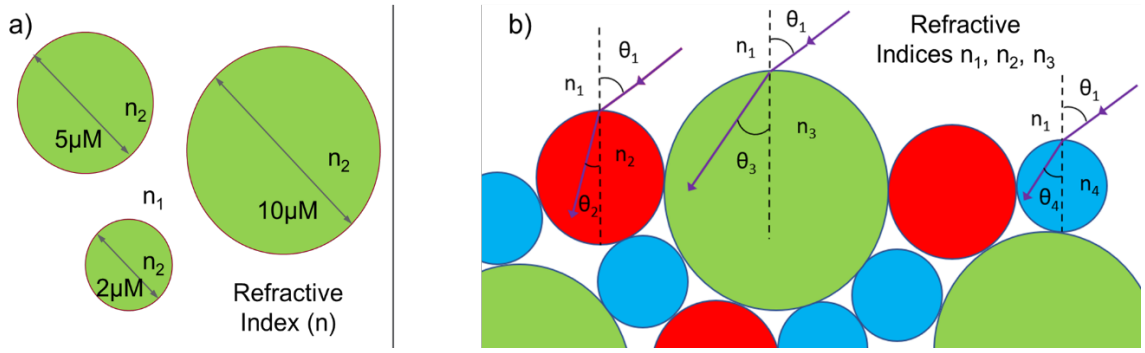

Figure 1. A schematic depicting the calculations needed for estimating the transmittance spectra for an ensemble of different size particles in a) the case of liquid droplets of the same medium (i.e., the same refractive index); and b) the case of particles of different liquids, (i.e., different refractive indices). For liquids with larger *k*-values, longer optical paths correspond to greater attenuation at those wavelengths.

2.0 Experimental

Briefly, the *n/k* optical constants are measured in the laboratory using standardized spectroscopic methods on bulk materials. A Fourier transform infrared (FTIR) spectrometer is used to make the spectroscopic measurements. [18, 19] Many of the methods have been either developed or improved upon at PNNL. For solids, [20-23] the delivered *n/k* data typically cover the wavenumber range 7500 to 400 cm^{-1} (1.33 to 25.0 μm), and for liquids, [24, 25] the delivered *n/k* data typically cover the wavenumber range 10,000 to 400 cm^{-1} (1.00 to 25.0 μm).

2.1 Liquids

The liquid optical constant data are measured from 10,000 to 400 cm^{-1} using methods adapted from Bertie and colleagues, [24 and references therein]. For each liquid, 6 to 10 absorption spectra are recorded with different optical path lengths by filling cells of various thicknesses. Using only signals that are a) above the spectrum noise floor and b) within the range of spectrometer linear response, a composite spectrum is derived. From this composite absorbance spectrum, the *n/k* vectors are calculated using the Kramers-Kronig transform (KKT). [20, 24] The KKT requires a known *n*-value for the liquid at the highest wavenumber (typically, 1 μm), which is obtained by fitting Abbe refractometer measurements collected at multiple visible wavelengths and at 1.55 μm. Figure 2 illustrates the experimental equipment and process for measuring the *n/k* spectra of a liquid.

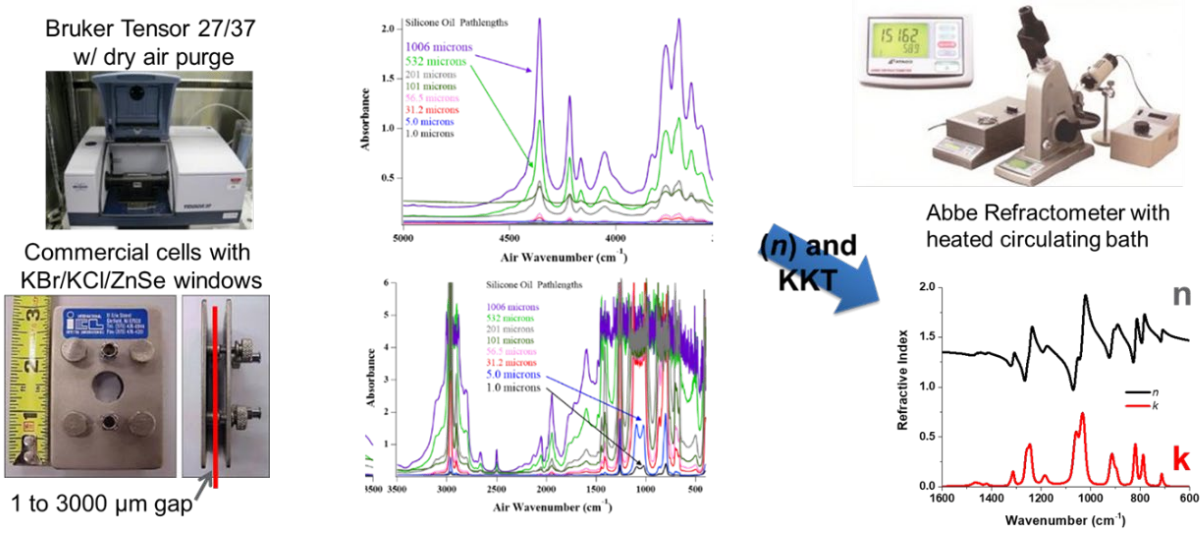

Figure 2. Liquid absorbance spectra are measured using a Fourier transform infrared spectrometer (upper left) with the liquid placed in transmission cells of different path lengths (lower left). Absorbance spectra of silicone oil in two different wavenumber ranges are shown (middle). From these absorbance spectra, a composite *k* spectrum is calculated. Using a refractometer (upper right), an *n* value of the liquid at the highest wavenumber is determined, and this, along with the *k* spectrum is used to calculate the *n* spectrum (lower right).

To cover the entire 10,000 to 400 cm^{-1} range, the FTIR is configured in two ways: the 10,000 to 4000 cm^{-1} near-infrared (NIR) range was measured with the FTIR using a Ge/CaF_2 beamsplitter, quartz-tungsten bulb, and DLaTGS room temperature infrared detector whereas the 7800 to 400 cm^{-1} mid-infrared range (MIR) was measured with a different FTIR using a Ge/KBr beamsplitter, silicon carbide heating element as the infrared source, and also a DLaTGS room temperature infrared detector. [25, 26] Figure 3 shows an overlap region for the two instrument configurations for the same 500 µm cell filled with 3-bromotoluene. Note the improved signal-to-noise for the NIR spectrum in this range. [26]

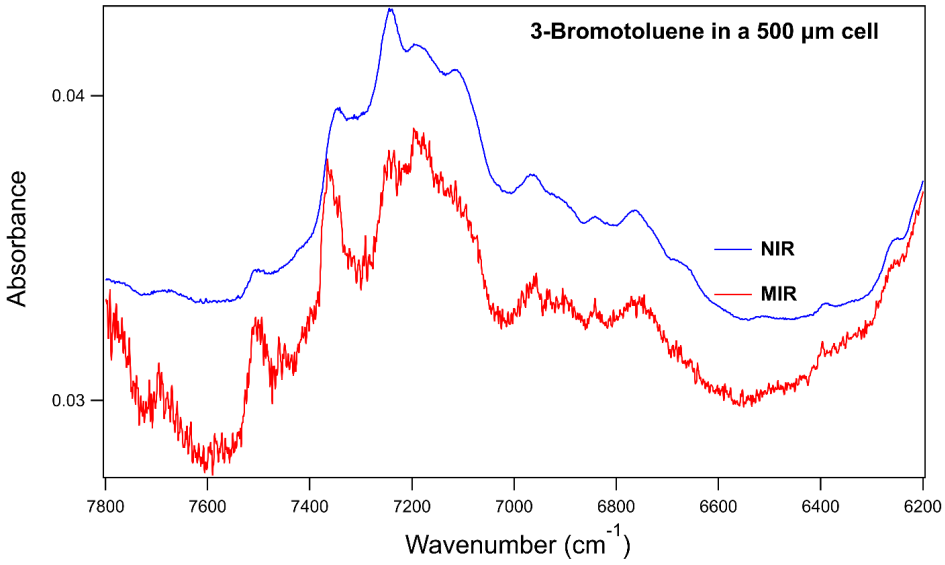

Figure 3. Absorbance spectra of 3-bromotoluene measured with a 500 µm cell and instruments configured for the NIR (top trace) or MIR (bottom trace) spectral range. Only the NIR data are used in this spectral region to provide good SNR. Spectra are vertically offset for clarity.

2.2 Solids

For solids, three methods can be used to measure the *n*/*k* vectors, sometimes using a combination of two different experimental methods for these pure materials. See Figure 4 for the instrumentation used in these three methods. In the first method, [27, 28] a variant of the KBr pellet absorption method is employed where a gravimetrically quantitative pellet is prepared. The analyte, < 1% by mass, is mixed into KBr powder, and the mixture pressed into a pellet using a die and hydraulic press. The quantitative absorption spectrum of a pellet of known size and mass is measured, and the values are derived from the measure absorbance, $A_{10}(\tilde{\nu}) = -\log_{10}\left(\frac{I(\tilde{\nu})}{I_0(\tilde{\nu})}\right)$, as detailed below.

The second measurement technique [29, 30] is the single angle (SA) reflectance method, where a quantitative reflectance spectrum is measured of the material at near normal (11°) incidence. In a few rare cases, single crystals of pure materials are available, but in most cases, the materials are organic powders that are ground into a fine powder and pressed into pellets, using a die and hydraulic press. The pellet is put at the focal point of the reflectance accessory, and the specular reflectance is measured relative to a 100% reflector, namely, first-surface gold. The *n*/*k* vectors are derived from these reflectance measurements (actually, a series of measurements over different spectral ranges are made) using the KKT. For quantitative results, this method requires optically smooth sample surfaces (*i.e.*, specular reflection rather than diffuse reflection).

The third method [14, 31] to obtain *n*/*k* solid materials is more time-consuming, so, it has largely been used as a corroborative method in the PICARD project. Rather than use the amplitude of reflected light as in the infrared SA method, IR spectroscopic ellipsometry (IRSE) uses polarizers and a rotating analyzer to measure the change in polarization of light reflected from a planar surface, both the phase and amplitude. From these measurements, an oscillator model of the sample material can be fitted to the ellipsometer data and from this the *n*/*k* optical vectors can be calculated.

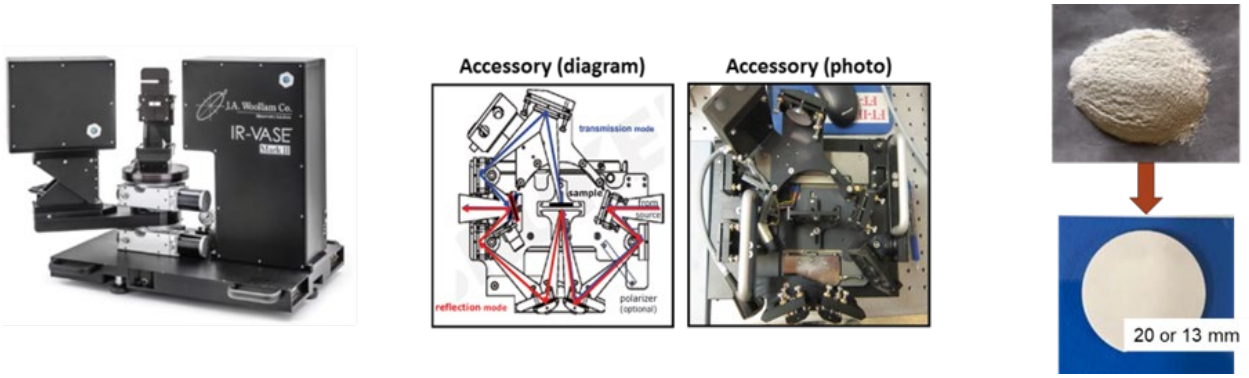

Figure 4. The infrared variable angle spectroscopic ellipsometer is shown on the left. The Bruker A510 single angle (11°) specular reflectance accessory, used for the single angle reflectance measurements, is shown in the middle two panels. A pelletized solid material is shown in the panel at the right. The material is ground and pressed into a pellet that is 13 or 20 mm in diameter.

3.0 Data Reduction

3.1 Liquids

The spectra are reduced using absorption data from different liquid cell path lengths to obtain values for the bands that are linear over several orders of magnitude and “stitching” the spectra together to make a composite spectrum. Silicone oil is used as an example (see Figure 5). [26]

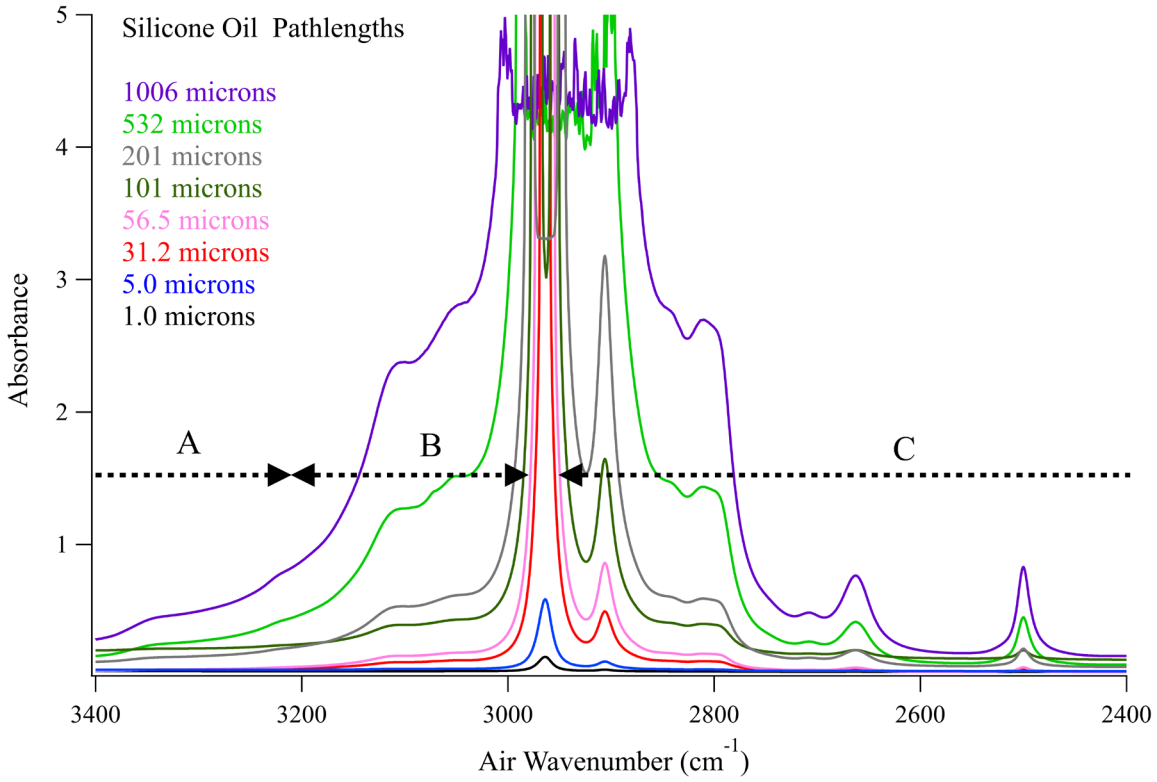

Figure 5. Multi-burden absorbance spectra (3400 - 2400 cm^{-1}) of silicone oil for varying cell path lengths (1 – 1006 μm). For the long path lengths, the data become nonlinear for A ~> 2. The dashed lines represent spectral regions where different cell path lengths were used to generate the composite spectrum.

For the liquids, the mid-infrared and near-IR spectra for the same species are concatenated and baseline-corrected to make a single spectrum. In addition to the FTIR data, values of the scalar refractive index are needed to calculate *n*/*k*. These data are obtained measuring the scalar *n*-value at seven wavelengths using notch filters (480, 486, 546, 589, 644, 656, 1550 nm) on an Abbe refractometer and fitting the data to a modified Sellmeier equation of form $n(\lambda) = A + \left(\frac{B}{\lambda^2 - C}\right)^{1/2}$ (see Fig. 6). [31]

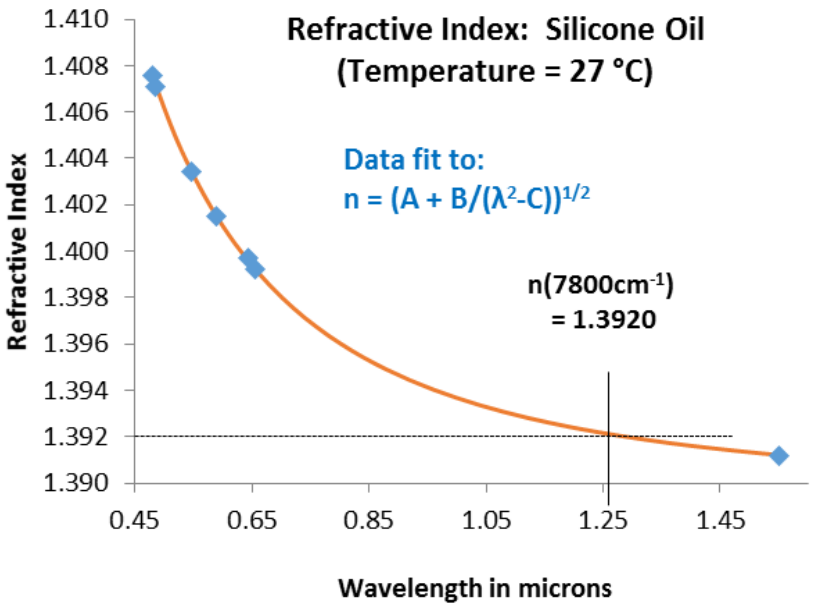

Figure 6. Plot of the measured refractive index values (blue symbols) versus the modified Sellmeier fit (orange trace) for silicone oil. The interpolated value at 7800 cm^{-1} (1.282 μm) is used as $n(\infty)$ in the KKT for the MIR data.

The $n(\lambda)$ is determined for the wavelength that represents the highest frequency measured in the FT spectra and is used as $n(\infty)$ in the KKT. The real optical constants $n(\tilde{\nu})$ are then obtained from the following equation where $\mathcal{P}$ is the Cauchy principal value.

$$n(\tilde{\nu}_i) = \frac{2}{\pi}\mathcal{P}\int_0^{\infty} \frac{\tilde{\nu}k(\tilde{\nu})}{\tilde{\nu}^2 - \tilde{\nu}_i^2} d\tilde{\nu} + n(\infty)$$

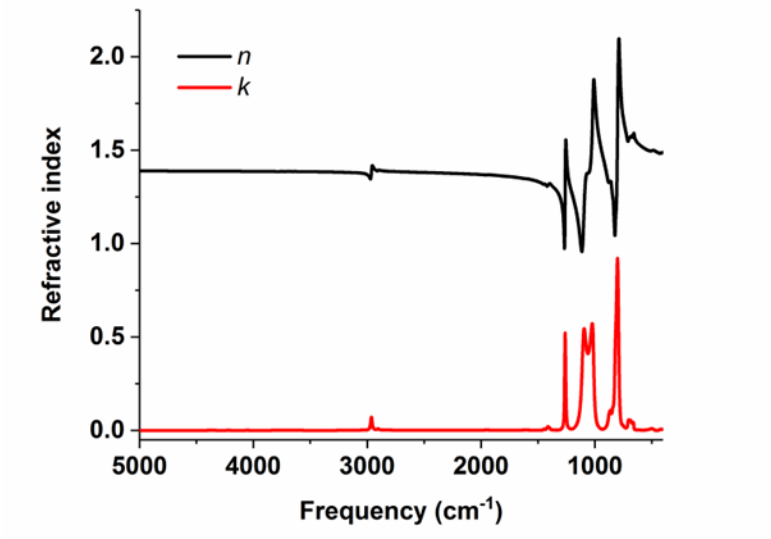

Figure 7. The final $n(\tilde{\nu})$ and $k(\tilde{\nu})$ vectors derived for silicone oil using 10 liquid cell path lengths ranging from 1 to 1006 μm.

Figure 7 shows the final $n(\tilde{\nu})$ and $k(\tilde{\nu})$ vectors for silicone oil in the MIR region. [25, 26, 31]. As described in reference [26], the composite MIR and NIR *k* vectors are merged around 3500 cm^{-1} to generate a final composite *k* vector across the entire spectral range (10,000 – 400 cm^{-1}). A weighted average, with the weight of the MIR vector increasing linearly from 0 to 100%, is used in the overlapping spectral region. The resulting composite *k* vector and the refractive index at 10,000 cm^{-1} are used to create the final *n* vector using the Kramers-Kronig relation, as per Bertie's program "LZZKTB."

3.2 Solids

For the solids, briefly, the data reduction steps for the KBr pellet method [27, 28] are:

1) Calculate the linear absorption coefficient: $K(\tilde{\nu}) = A(\tilde{\nu})/d$;
2) Calculate the imaginary refractive index: $k(\tilde{\nu}) = \frac{\ln(10)\cdot K(\tilde{\nu})}{4\cdot\pi\cdot\tilde{\nu}}$, and lastly
3) Calculate the real refractive index $n(\tilde{\nu})$ index from $k(\tilde{\nu})$ using the KKT.

The sample's effective thickness or optical depth is given as d = analyte mass/($\pi \bullet r^2 \bullet \rho$), where r is the radius of the pellet (0.65 cm), and ρ is the analyte density.

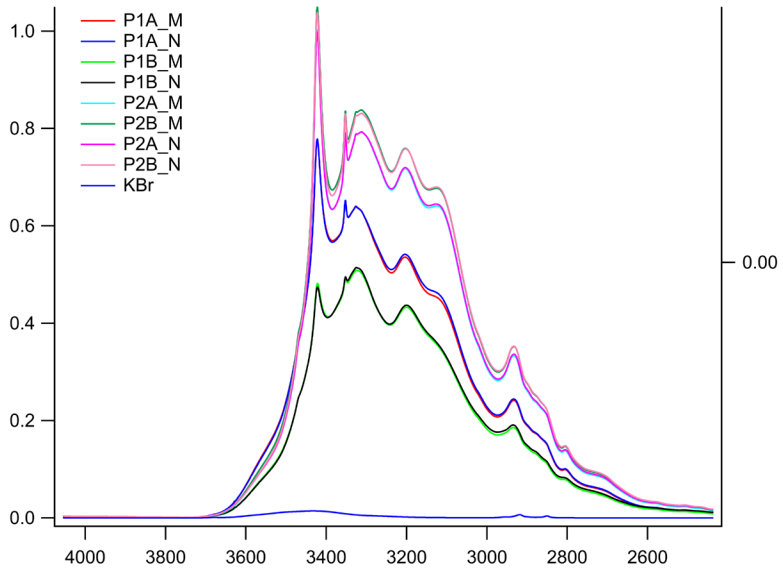

Figure 8. Plot of the absorption coefficient, $K(\tilde{\nu})$, for metformin calculated for four different KBr pellets (P1A, P1B, P2A and P2B) measured in the mid-infrared (_M) and the near-infrared (_N). The pure KBr pellet spectrum, which is used for subtraction, is also shown.

As an example of the KBr pellet method, we present the results for metformin. Two dilutions of metformin in KBr powder were prepared, and from these dilutions four pellets were made, each

with a different optical depth as seen in Table 1. The absorbance spectra of all four pellets were measured in both the MIR and NIR. See Figure 8.

Table 1. Pellets prepared in KBr for measurements of metformin.

Pellet #	Mass (g)	Optical Depth (μm)
Metformin Dilution #1: 0.18% metformin in KBr		
P1A	0.2708	2.832 μm
P1B	0.1945	2.034 μm
Metformin Dilution #2: 0.39% metformin in KBr		
P2A	0.1808	4.051
P2B	0.1903	4.263

Next, a $k(\tilde{\nu})$ vector is calculated from each absorbance spectrum, $K(\tilde{\nu})$, using the formula given above, and these $k(\tilde{\nu})$ vectors are then averaged. Finally, the $n(\tilde{\nu})$ vector is calculated from the $k(\tilde{\nu})$ using Bertie's LZZKTB program, and assuming the real index, n at 7800 cm^{-1} is 1.53. [24] The final $n(\tilde{\nu})$ and $k(\tilde{\nu})$ vectors for metformin, as determined from the KBr pellet method, are plotted in Figure 9.

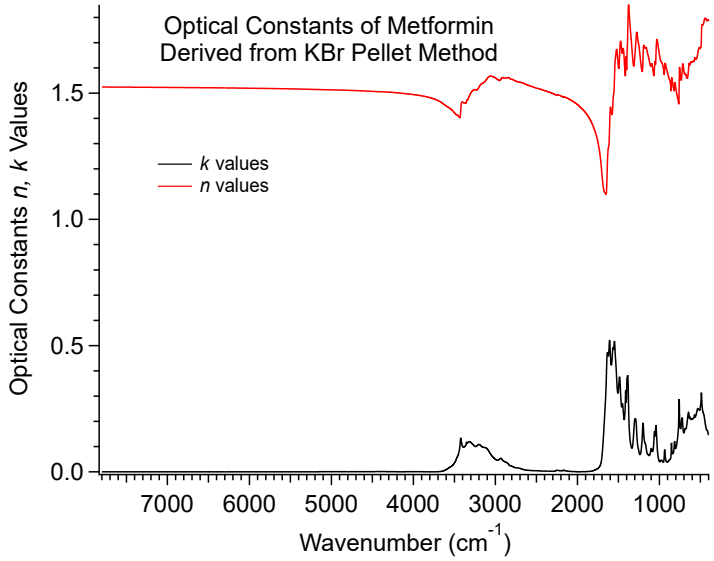

Figure 9. The calculated infrared optical constants for metformin are shown. The optical constants were determined by measuring the absorbance spectra of metformin-in-KBr pellets, calculating a *k* spectrum, and then using the KKT to calculate *n*.

Determining the *n*/*k* vectors for solids using the single angle method begins with measuring the absolute reflectance $R(\tilde{\nu})$ of the air/sample edge (vertical incidence). [29, 30] The reflectance is given by the Fresnel equation, [20, 31]

$$R(\tilde{\nu}) = |[n(\tilde{\nu}) - 1] / [n(\tilde{\nu}) + 1]|^2.$$

The real (*n*) and the imaginary (*k*) parts of the refractive index are calculated from the following expressions:

$$n(\tilde{\nu}) = [1 - R(\tilde{\nu})] / [1 + R(\tilde{\nu}) - 2R^{½}(\tilde{\nu})\cos(\varphi(\tilde{\nu}))] \text{ and}$$

$$k(\tilde{\nu}) = 2R^{½}(\tilde{\nu})\sin(\varphi(\tilde{\nu})) / [1 + R(\tilde{\nu}) - 2R^{½}(\tilde{\nu})\cos(\varphi(\tilde{\nu}))]$$

The phase angle, $\varphi(\tilde{\nu})$, is determined from the KKT. [20, 31] As an example, the reflectance spectrum of UV-grade fused silica is shown in Figure 10. The spectrum was measured using the Bruker A510 single angle reflectance accessory. A KBr beamsplitter was used to measure the reflectance spectrum from 7500 to 400 cm^{-1}, and a Mylar beamsplitter was used to measure the spectrum from 600 to 65 cm^{-1}. These spectra were merged, and the baseline of the reflectance spectrum was extrapolated from 65 to 0 cm^{-1}.

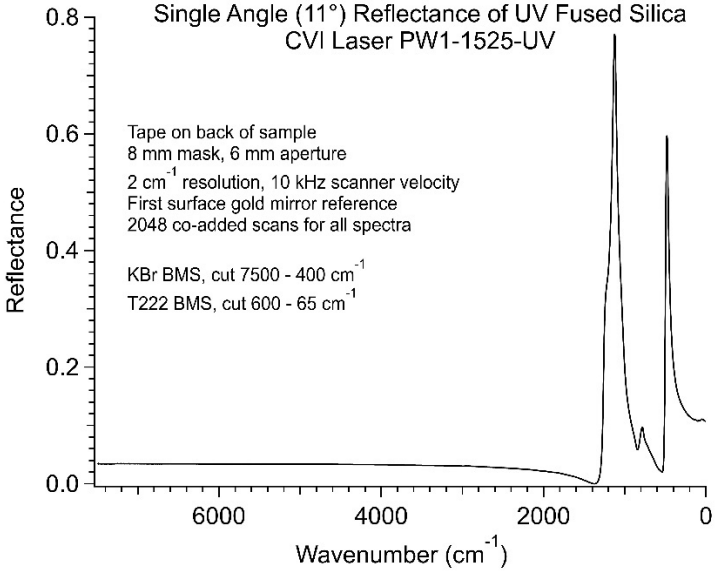

Figure 10. The reflectance spectrum of a UV-grade, fused silica window (CVI Laser Optics, Inc. part number PW1-1525-UV) is shown.

The $R(\tilde{\nu})$ spectrum, nominally from zero to infinity wavenumbers, is used in the KKT to generate the *n*/*k* vectors as seen in Fig. 11.

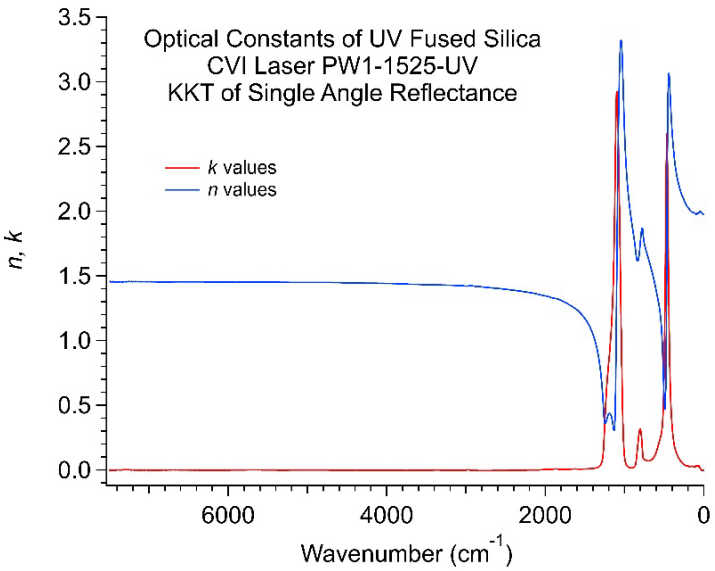

Figure 11. The *n*/*k* vectors shown in the plot were generated by performing a Kramers-Kronig transform on the reflectance spectrum shown in Fig. 10.

When possible, the *n*/*k* vectors derived by the various methods are vetted against one another. Figure 12 compares the *n/k* vectors of the UV-grade fused silica sample as measured by the single angle reflectance technique and infrared variable angle spectroscopic ellipsometry.

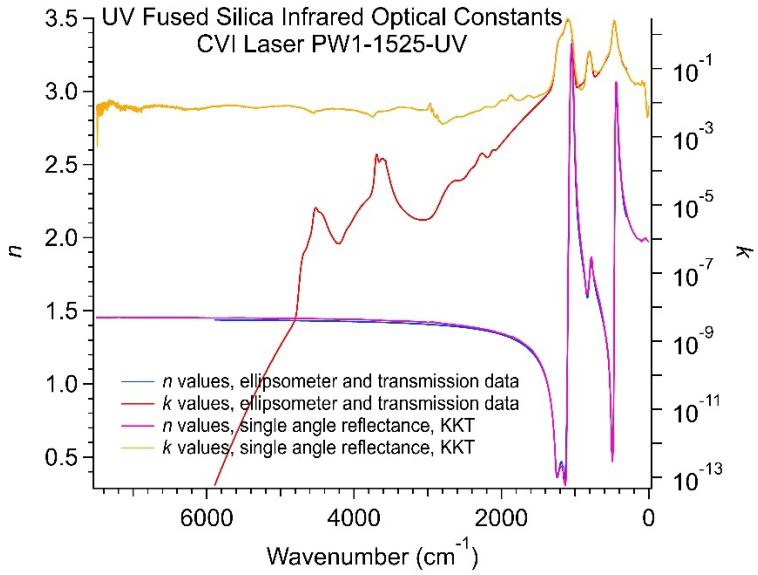

Figure 12. Plot of the *n/k* vectors for UV-grade fused silica as determined from single angle reflectance and variable angle spectroscopic ellipsometry. The *n* vectors (left axis linear scale; blue and pink traces) show excellent agreement. The *k* vectors (right axis logarithmic scale; red and orange traces) show excellent agreement below 1800 cm^{-1} for larger *k* values. The ellipsometry technique is more sensitive to weaker *k* values and structure in the *k* vector above 1800 cm^{-1}.

Figure 12 shows there is excellent agreement between the single angle reflectance and ellipsometry techniques for determining the *n* values for the fused silica sample. For this sample, the *k* values below 1800 cm^{-1} from the two techniques also show good agreement; however, the ellipsometer signal is averaged over several days, compared to several hours for the single angle reflectance technique, allowing observation of the weak *k* values above 1800 cm^{-1}.

4.0 Results

4.1 Optical Modeling

This section provides a description of how the measured *n/k* data described in Section 3.0 are used to model infrared light interactions with aerosols. [15, 16, 17, 32, 33]

Advancing the ability to detect aerosols through optical methods requires a comprehensive library of reference spectra that captures how particles transmit, reflect, and scatter light. These spectra must span the diversity of aerosol populations, accounting for variations in particle size, chemical composition, and concentration. PNNL has developed software that simulates the scattering, transmission (T), and absorption (A) properties of aerosols in the infrared, not only for the species of interest but also for common background materials such as water or solid particulates (e.g., carbon soot) that can act as condensation surfaces. [15-17, 33] Since the interaction of light (as a function of wavelength) with aerosols depends on the particle geometry, spectra were modeled for discrete particle sizes (e.g., 1, 2, 5, 10… µm) using a distribution (spanning 0.5 to 100 µm) typically observed in plumes. [15, 33] In addition to different sizes, the model can also accommodate mixed chemical species with their characteristic refractive indices.

This modeling requires the complex refractive index data for each chemical species; thus, the requisite *n*/*k* data for these species will be recorded using “gold-standard” protocols [13, 14, 25-30] developed at PNNL for many chemicals that have not been previously measured but have been identified as a material of interest for the PICARD program. Using the Fresnel equations, [20, 30] which require the chemicals’ complex refractive indices as input, the wavelength-dependent absorption and scattering of the IR light for the given collection of particles can be calculated. This will enable the ability to monitor and detect multiple threat agents, for example chemical warfare agents (CWAs) and pharmaceutical-based agents (PBAs) in both the aerosol and gas phases, including their detection in complex environments. [15, 33-35]

For the optical modeling effort, PNNL has written [15-17, 33] a MATLAB script built around an online MATLAB package developed by Shafer [36] to generate transmittance, scattering and absorption spectra from computed cross sections for single particles and particle ensembles. Briefly, this script calculates the scattering and absorption cross sections for a spherical particle of a specified chemical at each wavelength using the chemical’s refractive index producing single particle “cross section spectra”. [15-17, 33] This spectral computation is iterated over each particle size using the input particle diameter distribution, and the spectrum for each diameter is scaled

by its corresponding number concentration. The contributions from each particle size are then summed to give the wavelength-dependent particle ensemble absorption and scattering cross sections. Synthetic spectra are generated using a MATLAB script (with .txt input and output files). [15-17, 33] PNNL has incorporated geometrical parameters for experimental conditions (e.g., light source cross sectional area, plume dimensions, detector position) to compute absorption, scattering or transmission spectra in the script.

Finite Difference Time Domain (FDTD) calculations (see Figure 13) are also used to predict cross sections for single particles to validate the Mie scattering predictions from our MATLAB script. [15-17, 33] Since FDTD computes an exact solution to Maxwell's equations for an input model system, it cannot realistically be used for particle ensemble predictions. However, FDTD can handle a larger range of particle diameters, including sub-wavelength sizes which are not accurately treated with Mie theory alone, as well as aspherical and non-uniformly composed particle types. As seen in Figure 13, the shapes of features in the spectra vary slightly between particle calculations, but the peak positions do not, showing identical 150-200 nm shifts compared to the slab transmittance bands at 7.85 and 8.85 μm. [15] Agreement between the calculations will allow us to more efficiently model particle ensembles by using our Mie scattering software rather than a far more computationally expensive FDTD approach. [15-17, 33]

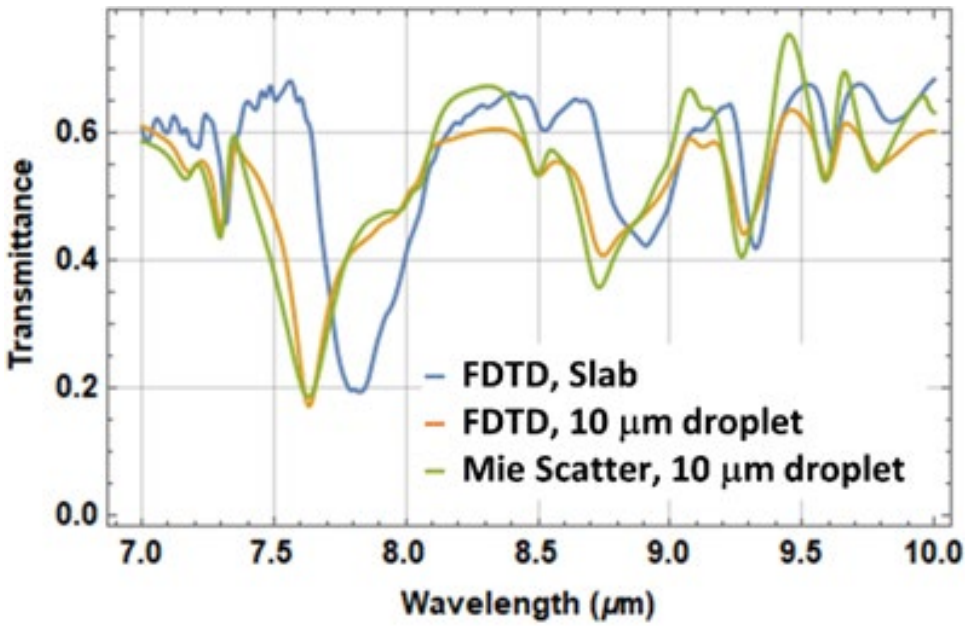

Figure 13. Predicted transmittance from 7 to 10 μm for a 10 μm particle of diethyl phthalate (DEP) using finite difference time domain (FDTD) (orange) and the PNNL Mie scattering-based software (green) compared to a 10 μm slab of DEP (blue).

Building on the momentum from our method validation success, work also began on optical modeling of particle ensembles for spherical single chemical aerosols. The optical constants of liquid dioctyl sebacate (DOS) were derived using the methods described in earlier sections (see Figure 14). [33] Separately, the particle diameter distribution of a lab-generated (nebulized) aerosol of DOS was measured by both an aerodynamic (APS) and optical (OPS) particle sizer. These optical constants and the measured particle size distributions were then input to the modified Mie scattering-based MATLAB code to predict transmission spectra for the lab-generated aerosol (see Figure 15). [15-17, 33]

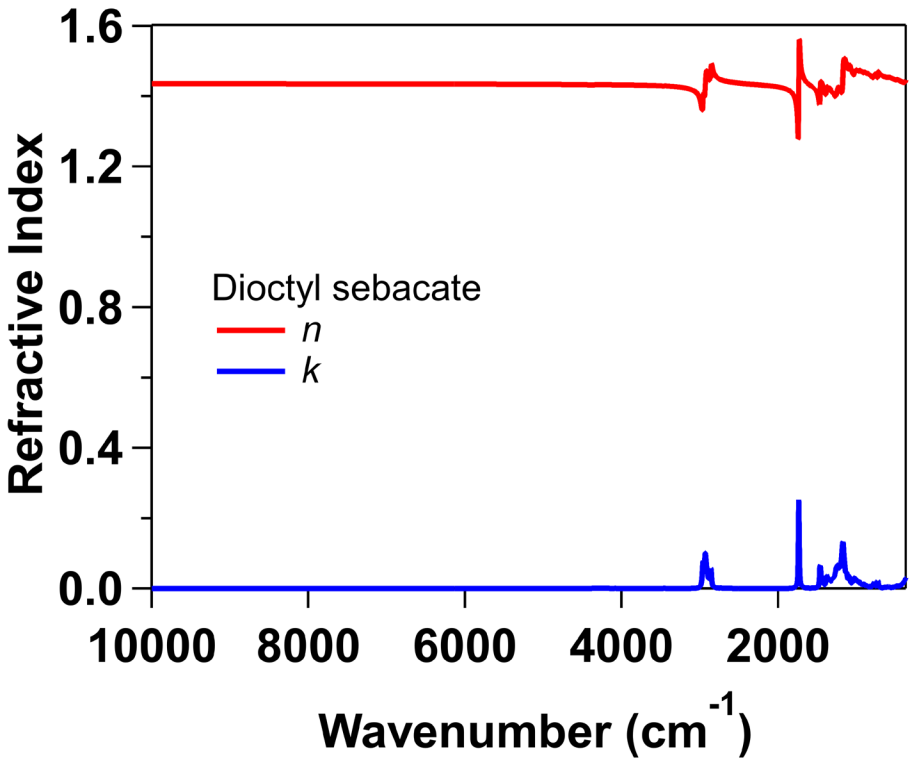

Figure 14. Optical constants for liquid dioctyl sebacate with the *k* (imaginary) and *n* (real) values plotted on same axis from 10,000 – 400 cm^{-1} (1 – 25 μm).

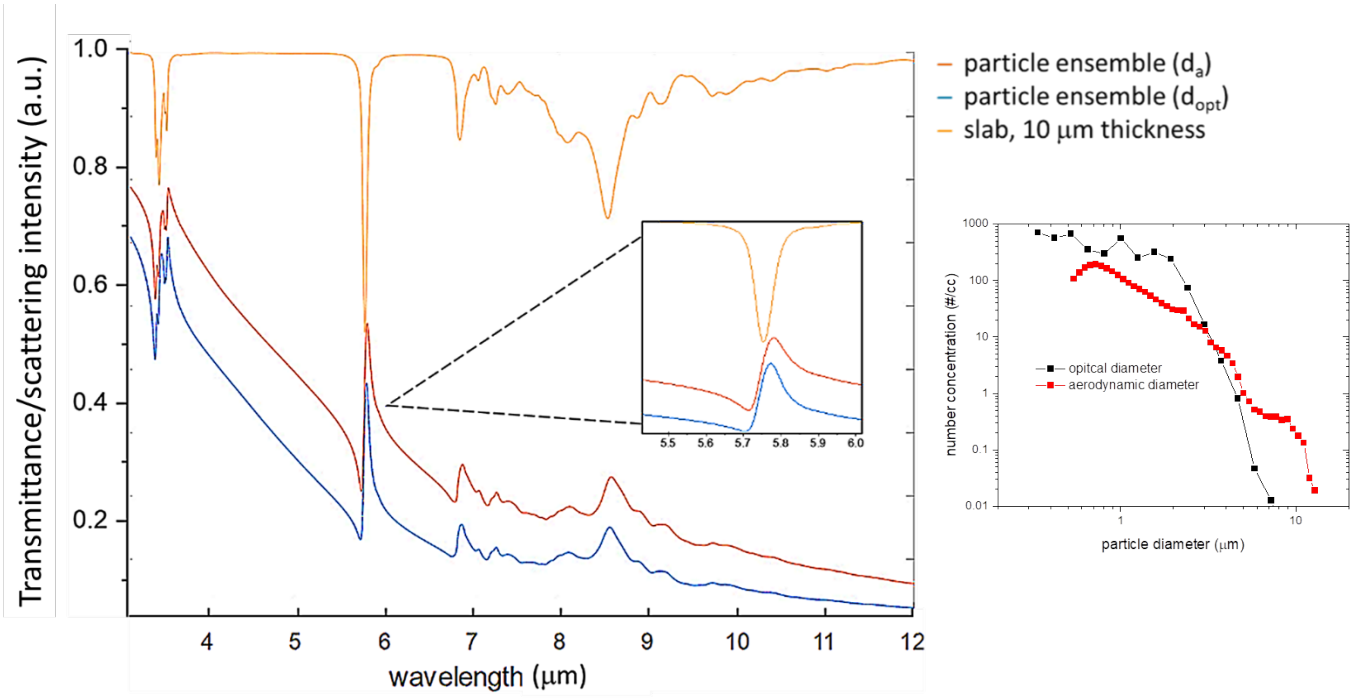

Figure 15. Left: Modeled total scattered light intensity using aerodynamic (red) or optical (blue) particle diameter distributions for the nebulized DOS aerosol sample compared to transmittance for a 10 μm slab (orange). Right: Aerodynamic (red) and optical (black) particle diameter distributions for a nebulized dioctyl sebacate DOS aerosol sample.

It is noteworthy here that the shifts in most features relative to slab transmittance are small (~50 nm), especially compared to the spectral shifts (~200 nm) seen in modeled transmission spectra for aerosol particles of other compounds, for example, diethyl phthalate (DEP). The differences in the two measured particle diameter distributions also produce very small shifts in band positions relative to each other (~10 nm). This represents the first “test” for our software modeling a particle ensemble and enables future comparison to real world aerosol IR transmission measurements. [15-17, 33]

5.0 Deliverable

PNNL has delivered to the PICARD program a set of *n/k* data for each of the target chemicals, 72 liquids and 42 solids (see Table 2). Each one of these data sets contains the *n* and *k* vectors for the chemical of interest. The data were delivered as a three-column set where the first column is the wavenumber (cm^{-1}), the second column is the *n* value at that wavenumber, and the third column is the *k* value (proportional to the absorption coefficient), that is the imaginary component of the refractive index at that wavenumber. These data sets are self-contained and have continuous spectrum coverage that typically span 10,000 to 400 cm^{-1} (1.00 to 25.0 µm) for liquids and 7800 cm^{-1} to 400 cm^{-1} (1.282 to 25.0 µm) for solids.

Table 2. PICARD chemical list for *n*/*k* measurements.

Sample Name (library name)	CAS #	State
1,1,3,3-Tetramethylguanidine	80-70-6	Liquid
1,4-Butanediol	110-63-4	Liquid
1-Benzyl-4-piperidone	3612-20-2	Liquid
1-Octanol	111-87-5	Liquid
2,3-Butanediol	513-85-9	Liquid
2-Chloroethyl ethyl sulfide (CEES)	693-07-2	Liquid
2-Ethylhexyl acrylate	103-11-7	Liquid
4-Amino-1-benzyl piperidine	50541-93-0	Liquid
4-Carvomenthenol	562-74-3	Liquid
4-Methyl-2-pentanone	108-10-1	Liquid
4-Methylpyridine	108-89-4	Liquid
6-Methyl-2-heptanone	928-68-7	Liquid
Acetophenone	98-86-2	Liquid
Ammonium hydroxide solution (aqueous)	1336-21-6	Liquid
Aniline	62-53-3	Liquid
Anisole	100-66-3	Liquid
Benzaldehyde	100-52-7	Liquid
Chloroacetone	78-95-5	Liquid
Cyclohexanol	108-93-0	Liquid
Dibutyl phthalate	84-74-2	Liquid
Diethyl malonate	105-53-3	Liquid
Diethyl methyl phosphonate (DEMP)	683-08-9	Liquid
Diethyl phosphite	762-04-9	Liquid
Diethyl phthalate	84-66-2	Liquid
Diethyl sebacate (DES)	110-40-7	Liquid
Diisopropyl methyl phosphonate (DIMP)	1445-75-6	Liquid
Dimethyl methylphosphonate (DMMP)	756-79-6	Liquid
Dimethyl sulfoxide (DMSO)	67-68-5	Liquid

Dioctyl sebacate (bis-2-ethylhexyl sebacate)	122-62-3	Liquid
Ethanol	64-17-5	Liquid
Ethyl 2-cyanoacrylate	7085-85-0	Liquid
Ethyl benzene	100-41-4	Liquid
Ethyldiethanolamine	139-87-7	Liquid
Ethylene glycol	107-21-1	Liquid
Furfurylamine	617-89-0	Liquid
Glycerol	56-81-5	Liquid
Isoamyl acetate	123-92-2	Liquid
Isopropyl Alcohol (2-propanol)	67-63-0	Liquid
Malathion	121-75-5	Liquid
Mecrylate (methyl 2-cyanoacrylate)	137-05-3	Liquid
Methanol	67-56-1	Liquid
Methyl caprate (methyl decanoate)	110-42-9	Liquid
Methyl diethanolamine (MDEA)	105-59-9	Liquid
Methyl laurate	111-82-0	Liquid
Methyl paraoxon	950-35-6	Liquid
Methyl salicylate	119-36-8	Liquid
Methyl undecanoate	1731-86-8	Liquid
n-Butyl mercaptan (1-butanethiol)	109-79-5	Liquid
Nitrobenzene	98-95-3	Liquid
N,*N*-Diethylaniline	91-66-7	Liquid
n-Octane	111-65-9	Liquid
Oleic acid	112-80-1	Liquid
o-Xylene	95-47-6	Liquid
Parathion	56-38-2	Liquid
Permethrin	52645-53-1	Liquid
Phenethylamine	64-04-0	Liquid
Pinacolone (3,3-dimethyl-2-butanone)	75-97-8	Liquid
Pinacolyl Alcohol (3,3-dimethyl-2-butanol)	464-07-3	Liquid
Pinonaldehyde	2704-78-1	Liquid
Propylene glycol	57-55-6	Liquid
Safrole	94-59-7	Liquid
Tetraethylene glycol dimethyl ether	143-24-8	Liquid
Thiodiglycol (2.2-thiodiethanol)	111-48-8	Liquid
Toluene	108-88-3	Liquid
Tributyl phosphate (TBP)	126-73-8	Liquid
Triethanolamine	102-71-6	Liquid
Triethyl phosphate (TEP)	78-40-0	Liquid
Triisopropyl phosphate	513-02-0	Liquid
Trimethyl phosphate	512-56-1	Liquid
Trimethylbenzene (Mesitylene)	108-67-8	Liquid
Tris(2-ethylhexyl)phosphate	78-42-2	Liquid
Tropane	529-17-9	Liquid

1,1-Dimethylbiguanide (Metformin)	657-24-9	Solid
2,4,5-Trichlorophenol	95-95-4	Solid
2,4-Dinitrophenol	51-28-5	Solid
2,4-Dinitrotoluene - DNT isomers	121-14-2	Solid
3-Nitroaniline	99-09-2	Solid
4,6-Dinitro-m-xylene	616-72-8	Solid
4-Aminopyridine	504-24-5	Solid
Acetaminophen, Paracetamol	103-90-2	Solid
Acetylsalicylic acid	50-78-2	Solid
Anthranilic acid	118-92-3	Solid
Arachidic acid	506-30-9	Solid
CaCO3	471-34-1	Solid
Caffeine	58-08-2	Solid
Camphor (2-bornanone)	76-22-2	Solid
Cellulose	9004-34-6	Solid
Chitosan	9012-76-4	Solid
Dextrose (d-+-glucose)	50-99-7	Solid
Dicumylperoxide	80-43-3	Solid
Diuron	330-54-1	Solid
Eicosane	112-95-8	Solid
Fluoranthrene	206-44-0	Solid
Glyphosate	1071-83-6	Solid
Hexamine	100-97-0	Solid
HMX	2691-41-0	Solid
Indole	120-72-9	Solid
Lactofen	77501-63-4	Solid
Lactose	63-42-3	Solid
Mannitol	69-65-8	Solid
Metamizole sodium salt	68-89-3	Solid
Naphthalene	91-20-3	Solid
Nitrocellulose	9004-70-0	Solid
o-Chlorobenzylidenemalonitrile	2698-41-1	Solid
PETN	78-11-5	Solid
Phenanthrene	85-01-8	Solid
Phenol	108-95-2	Solid
Phloroglucinol	108-73-6	Solid
Sucrose	57-50-1	Solid
L-+-Tartaric acid	133-37-9	Solid
DL-Tartaric acid	87-69-4	Solid
TiO_2 (88% anatase, 12% rutile)	13463-67-7	Solid
TiO_2 (100% rutile)	1317-80-2	Solid
Xylazine	7361-61-7	Solid

The final data for many of the liquids measured under PICARD have also been posted to an open-source repository and are available for download. [37]

6.0 References

1. TJ Johnson, TL Myers and A Zelenyuk-Imre. 2023. "PNNL Capabilities for the PICARD Project." Client presentation, July 2023.

2. NA Macleod, F Molero and D Weidmann. 2015. "Broadband Standoff Detection of Large molecules by Mid-Infrared Active Coherent Laser Spectrometry." *Optics Express* 23(2):912-928. https://doi.org/10.1364/OE.23.000912.

3. L Maidment, Z Zhang, CR Howle and DT Reid. 2016. "Stand-Off Identification of Aerosols Using Mid-Infrared Backscattering Fourier-Transform Spectroscopy." *Optics Letters* 41(10):2266-2269. http://dx.doi.org/10.1364/OL.41.002266.

4. JA Huffman, AE Perring, NJ Savage, B Clot, B Crouzy, F Tummon, O Shoshanim, B Damit, J Schneider, V Sivaprakasam, MA Zawadowicz, I Crawford, M Gallagher, D Topping, DC Doughty, SC Hill and Y Pan. 2020. "Real-Time Sensing of Bioaerosols: Review and Current Perspectives." Aerosol Science and Technology, 54(5):465-495. https://doi.org/10.1080/02786826.2019.1664724.

5. J Li, Z Yu, Z Du, Y Ji and C Liu. 2020. "Standoff Chemical Detection Using Laser Absorption Spectroscopy: A Review." *Remote Sensing* 12:2771(1-44). https://doi.org/10.3390/rs12172771.

6. MK Jindal, M Mainuddin, S Veerabuthiran and AK Razdan. 2021. "Laser-Based Systems for Standoff Detection of CWA: A Short Review." *IEEE Sensors Journal* 21(4):4085-4096. https://doi.org/10.1109/JSEN.2020.3030672.

7. LM Narlagiri, MSS Bharati, R Beeram, D Banerjee and VR Soma. 2022. "Recent Trends in Laser-Based Standoff Detection of Hazardous Molecules." *Trends in Analytical Chemistry* 153:116645. https://doi.org/10.1016/j.trac.2022.116645.

8. OB Toon, JB Pollack and BN Khare. 1976. "The Optical Constants of Several Atmospheric Aerosol Species Ammonium Sulfate, Aluminum Oxide, and Sodium Chloride." *Journal of Geophysical Research* 81(33):5733-5748. https://doi.org/10.1029/JC081i033p05733.

9. J Li, JGD Wong, JS Dobbie and P Chylek. 2001. "Parameterization of the Optical Properties of Sulfate Aerosols." *Journal of the Atmospheric Sciences* 58(2):193-209. https://doi.org/10.1175/1520-0469(2001)058%3C0193:POTOPO%3E2.0.CO;2.

10. M Segal-Rosenheimer, Y Dubowski and R Linker. 2009. "Extraction of optical constants from mid-IR spectra of small aerosol particles." *Journal of Quantitative Spectroscopy & Radiative Transfer* 110(6-7):415–426. https://doi.org/10.1016/j.jqsrt.2009.01.005.

11. LM Ruan, XY Wanga, H Qi and SG Wanga. 2011. "Experimental Investigation on Optical Constants of Aerosol Particles." *Journal of Aerosol Science* 42(11):759–770. https://doi.org/10.1016/j.jaerosci.2011.07.001.

12. O Laskina, MA Young, PD Kleiber and VH Grassian. 2014. "Infrared Optical Constants of Organic Aerosols: Organic Acids and Model Humic-Like Substances (HULIS)." *Aerosol Science and Technology*, 48(6):630-637. https://doi.org/10.1080/02786826.2014.904499.

13. TJ Johnson, E Diaz, KD Hughey, TL Myers, TA Blake, AC Dohnalkova and SD Burton. 2020. "Infrared Optical Constants from Pressed Pellets of Powders: I. Improved *n* and *k* Values of $(NH_4)_2SO_4$ from Single-Angle Reflectance." *Applied Spectroscopy* 74(8):851–867. https://doi.org/10.1177/0003702820930009.

14. TL Myers, TA Blake, MO Yokosuk, G Fortin and TJ Johnson. 2020. "Improved Infrared Optical Constants from Pressed Pellets: II. Ellipsometric *n* and *k* Values for Ammonium Sulfate with Variability Analysis." *Applied Spectroscopy* 74(8):868–882. https://doi.org/10.1177/0003702820928358.

15. SP Lockwood, BE Bernacki, MJ Wilhelm, TL Myers, TJ Baker and TJ Johnson. 2024. "Modeling Aerosol Transmission Spectra from *n*(λ) and *k*(λ) Infrared Optical Constants Measurements of Organic Liquids and Solids." *Optics Express* 32(17):30169-30181. https://doi.org/10.1364/OE.529439.

16. D Cancino, JD Erickson, TJ Johnson and T.L. Myers. 2025. "Spectral Reflectance of Common Surfaces for (Laser) Detection of Aerosols and Gases." In *SPIE Defense + Commercial Sensing: Chemical, Biological, Radiological, Nuclear, and Explosives (CBRNE) Sensing XXVI, April 13-17, 2025, Orlando, FL. Proceedings of the SPIE*, edited by JA Guicheteau, CR Howle and TL Myers, *Proc. of SPIE* Vol.13478, 134780B 2025. Bellingham, Washington: SPIE. PNNL-SA-210482. https://doi.org/10.1117/12.3054656.

17. JM Salcido, SP Lockwood, A Zelenyuk, TJ Baker, BE Bernacki, TJ Johnson, TL Myers. 2025. "Modeling and Validation of Infrared Transmission Through Aerosolized Materials Using the Complex Refractive Index Spectra." *Chemical, Biological, Radiological, Nuclear, and Explosives (CBRNE) Sensing XXVI*, edited by JA Guicheteau, CR Howle, TL Myers, *Proc. of SPIE* Vol. 13478,134780G 2025 Published by SPIE 0277-786X. PNNL-SA-210480. https://doi.org/10.1117/12.3054467.

18. PR Griffiths and JA de Haseth, *Fourier Transform Infrared Spectrometry* (Wiley, San Francisco, 2007). https://doi.org/10.1002/047010631X.

19. RJ Bell, *Introductory Fourier Transform Spectroscopy* (Academic Press, New York, 1972).

20. V Lucarini, JJ Saarinen, K-E Peiponen and EM Vartiainen. *Kramers–Kronig Relations in Optical Materials Research* (Springer-Verlag, New York, 2005). https://doi.org/10.1007/b138913.

21. RI Young. 1977. "Validity of the Kramers-Kronig Transformation Used in Reflection Spectroscopy." *Journal of the Optical Society of America* 67(4)520-523. https://doi.org/10.1364/JOSA.67.000520.

22. P Grosse and V Offermann. 1991. "Analysis of Reflectance Data Using the Kramers-Kronig Relations." *Applied Physics A* 52:138-144. https://doi.org/10.1007/BF00323731.

23. K Yamamoto and H Ishida. 1997. "Kramers-Kronig Analysis Applied to Reflection-Absorption Spectroscopy." *Vibrational Spectroscopy* 15:27-36. https://doi.org/10.1016/S0924-2031(97)00017-9.

24. JE Bertie, SL Zhang, CD Keefe. 1995. ‘‘Measurement and Use of Absolute Absorption Intensities of Neat Liquids.’’ *Vibrational Spectroscopy*. 8(2):215–229. https://doi.org/10.1016/0924-2031(94)00038-I.

25. TL Myers, RG Tonkyn, TO Danby, MS Taubman, BE Bernacki, JC Birnbaum, SW Sharpe and TJ Johnson. 2018. “Accurate Measurement of the Optical Constants *n* and *k* for a Series of 57 Inorganic and Organic Liquids for Optical Modeling and Detection.” *Applied Spectroscopy* 2018, 72(4):535–550. https://doi.org/10.1177/0003702817742848.

26. OM Primera-Pedrozo, RG Tonkyn, TJ Baker, SP Lockwood, AM Bradley, TJ Johnson and TL Myers. 2026. “Extension of Complex Refractive Index Measurements to the Near-Infrared for Liquids: Methodology and Uncertainty Analysis.” *Applied Spectroscopy* accepted. https://doi.org/10.1177/00037028251399225.

27. TL Myers, RM Francis, CA Banach, SD Burton, AM Oeck, TJ Johnson, R Furstenberg and CA Kendziora. 2019. “Obtaining the Complex Optical Constants *n* and *k* via Quantitative Absorption Measurements in KBr Pellets.” *Proceedings of SPIE* 11010:110100M. Chemical, Biological, Radiological, Nuclear, and Explosives (CBRNE) Sensing XX. https://doi.org/10.1117/12.2519503.

28. KA Peterson, RM Francis, CA Banach, AM Bradley, SD Burton, JD Erickson, SP Lockwood, KL Jensen, MO Yokosuk, TJ Johnson and TL Myers. 2024. “Method to Derive the Infrared Complex Refractive Indices *n*(l) and *k*(l) for Organic Solids from KBr Pellet Absorption Measurements.” *Applied Optics* 63(6):1553-1565. https://doi.org/10.1364/AO.514661.

29. BM DeVetter, NK Scharko, BD Cannon, TL Myers, and TJ Johnson. 2018. “Single-Angle Reflectance Spectroscopy to Determine the Optical Constants *n* and *k*: Considerations in the Far-Infrared Domain.” *Applied Optics* 57(22):6587-6597. https://doi.org/10.1364/AO.57.006587.

30. KA Peterson, BE Bernacki, DL Saunders, JD Erickson, SP Lockwood, TJ Johnson, TL Myers. 2024. “Deriving the Infrared Complex Refractive Indices of Organic Powders for Optical Modeling: Comparison of Methods.” *Proceedings of SPIE* 13031:130310E. Algorithms, Technologies, and Applications for Multispectral and Hyperspectral Imaging XXX, edited by Miguel Velez-Reyes, David W. Messinger. https://doi.org/10.1117/12.3013843.

31. H Fujiwara. *Spectroscopic Ellipsometry: Principles and Applications* (Wiley, San Francisco, 2007). https://doi.org/10.1002/9780470060193.

32. CF Bohren and DR Huffman. *Absorption and Scattering of Light by Small Particles* (Wiley, San Francisco, 1983). https://doi.org/10.1002/9783527618156.

33. JMO Salcido, SP Lockwood, A Zelenyuk, TJ Baker, BE Bernacki, TL Myers and TJ Johnson. 2025. “Quantitative Infrared Spectroscopy of Aerosols: Mie Theory Modeling with Experimental Validation.” *Optica* 12(9):1462-1468. https://doi.org/10.1364/OPTICA.566710.

34. D Khanal, J Zhang, W-R Ke, MMB Holl and H-K Chan. 2025. “Bulk to Nanometer-Scale Infrared Spectroscopy of Pharmaceutical Dry Powder Aerosols.” *Analytical Chemistry* 92(12):8323-8332. https://dx.doi.org/10.1021/acs.analchem.0c00729.

35. NE Olson, Y Xiao, Z Lei and AP Ault. 2020. “Simultaneous Optical Photothermal Infrared (O-PTIR) and Raman Spectroscopy of Submicrometer Atmospheric Particles.” *Analytical Chemistry* 92(14):9932-9939. https://dx.doi.org/10.1021/acs.analchem.0c01495.

36. J Shafer 2011. MatScat. https://www.mathworks.com/matlabcentral/fileexchange/36831-matscat. MATLAB Central File Exchange.

37. Tracy J. Baker, Ashley M. Bradley, Timothy J. Johnson, Tanya L. Myers, Oliva M. Primera-Pedrozo and Russell M. Tonkyn. 2025. PNNL LIQUIDS REFRACTIVE INDEX (*n*/*k*) DATASET FROM 1 TO 25 MICRONS. [Data Set] PNNL DataHub. https://doi.org/10.25584/2997107